Electrical polarization switching in bulk single-crystal $GaFeO_3$

Maria Biernacka,[1] Paweł Butkiewicz,[2] Konrad J. Kapcia,[3] Wojciech Olszewski,[1,*] Dariusz Satuła,[1] Marek Szafrański,[4] Marcin Wojtyniak,[5] and Krzysztof R. Szymański[1]

[1]*Faculty of Physics, University of Bialystok, Konstantego Ciolkowskiego 1L, 15-245 Białystok, Poland*

[2]*Doctoral School of Exact and Natural Sciences, University of Bialystok, Konstantego Ciolkowskiego 1K, 15-245 Białystok, Poland*

[3]*Institute of Spintronics and Quantum Information, Faculty of Physics, Adam Mickiewicz University in Poznań, Uniwersytetu Poznańskiego 2, 61-614 Poznań, Poland and Center for Free-Electron Laser Science CFEL, Deutsches Elektronen Synchrotron DESY, Notkestr. 85, 22607 Hamburg, Germany*

[4]*Faculty of Physics, Adam Mickiewicz University in Poznań, Uniwersytetu Poznańskiego 2, 61-614 Poznań, Poland*

[5]*Institute of Physics–Center for Science and Education, Silesian University of Technology, Krasińskiego 8, 40-019 Katowice, Poland*

(Received 17 July 2023; revised 22 September 2023; accepted 3 October 2023; published 1 November 2023)

The electrical polarization switching on a stoichiometric $GaFeO_3$ single crystal was measured, and a model of atomic displacements responsible for the polarization reverse was proposed. The widely adapted mechanism of polarization switching in $GaFeO_3$ can be applied to stoichiometric, perfectly ordered crystals. However, the grown single crystals, as well as thin films of Ga-Fe-O, show pronounced atomic disorder. Using piezoresponse force microscopy, the electrical polarization switching on a crystal surface perpendicular to the electrical polarization direction was demonstrated. Atomic disorder in the crystal was measured by x-ray diffraction and Mössbauer spectroscopy. These measurements were supported by *ab initio* calculations. Using analysis of atomic disorder and electronic structure calculations, the energies of defects of cations in foreign cationic sites were estimated. The energies of the polarization switch were estimated, confirming the proposed mechanism of polarization switching in $GaFeO_3$ single crystals.

DOI: 10.1103/PhysRevB.108.195101

I. INTRODUCTION

The $GaFeO_3$ compound crystallizes in the orthorhombic structure of space group $Pna2_1$ (No. 33). The asymmetric unit cell contains two nonequivalent iron (Fe1, Fe2), two gallium (Ga1, Ga2), and six oxygen sites. The symmetry operations acting on the atom at point (x, y, z) transform it into three other positions $(x + 1/2, -y + 1/2, z)$, $(-x, -y, z + 1/2)$, and $(-x + 1/2, y + 1/2, z + 1/2)$, yielding 40 atoms in the unit cell. $GaFeO_3$ is a polar compound, as the atomic positions for opposite polarities are shown schematically in Figs. 1 and 2. The cation in the Ga1 site has tetrahedral coordination, while in the remaining Ga2, Fe1, and Fe2 sites, cations are coordinated by distorted octahedra. It is well documented that single crystals obtained so far exhibit pronounced disorder between cationic sites. For example, Arima *et al.* [1] reported in their single crystal the site occupancies as follows: Ga1: 0.82Ga, 0.18Fe; Ga2: 0.65Ga, 0.35Fe; Fe1 0.23Ga 0.77Fe; Fe2: 0.30Ga, 0.70Fe. Using diffraction and Mössbauer experiments, it was shown that the iron occupancy of Ga tetrahedral sites is much lower than Ga octahedral sites [1–9]. Thus, one expects that iron in a tetrahedral site is energetically unfavorable. In fact, the hyperfine structure of the ^{57}Fe nuclear probe at that site is ambiguous because of the low area under the spectra and substantial line overlap. For example, quadrupole splitting for Fe in the Ga1 site was reported to be −0.07 [5] or 0.40(2) [6] (in mm/s).

Stoeffler proposed a model of atomic displacements realizing change between two polarization states of $Pna2_1$ structure of fully ordered $GaFeO_3$, $P_z > 0$ [Fig. 1(a)] and $P_z < 0$ [10] [Fig. 1(b)]. Switching between two polarization states can be realized by a shift of atoms shown schematically by arrows in Fig. 1. The maximal displacement of oxygen anions deduced from the literature (Table I) [10] is about 1.2 Å; therefore, it is expected that the switching of the electric polarization cannot be realized easily [11]. Moreover, the switching between two polarization states shown in Fig. 1 [10] changes the local atomic environments. For example, site Fe1 of state $P_z > 0$ changes into site Fe2 of state $P_z < 0$ (and site Fe2 of state $P_z > 0$ changes into site Fe1 of state $P_z < 0$). Similarly, site Ga1 of state $P_z > 0$ changes into site Ga2 of state $P_z < 0$ (and site Ga2 of state $P_z > 0$ changes into site Ga1 of state $P_z < 0$). However, switching between two polarization states proposed by Stoeffler [10] cannot be realized in the case of disordered crystals. As an illustration, let us consider the already mentioned crystal grown by Arima (Kaneko *et al.* [12]). By switching its polarization state, one would get the partial site occupancies: Ga1: 0.65Ga, 0.35Fe; Ga2: 0.82Ga, 0.18Fe; Fe1: 0.30Ga, 0.70Fe; Fe2: 0.23Ga 0.77Fe [1]. Thus, the two states ($P_z < 0$ and $P_z > 0$) would differ by atomic disorder and cannot be considered as two opposite polarization states of a ferroelectric. As was already argued, iron in the tetrahedral site is energetically unfavorable; thus, the two states would differ in energy.

*Corresponding author: w.olszewski@uwb.edu.pl

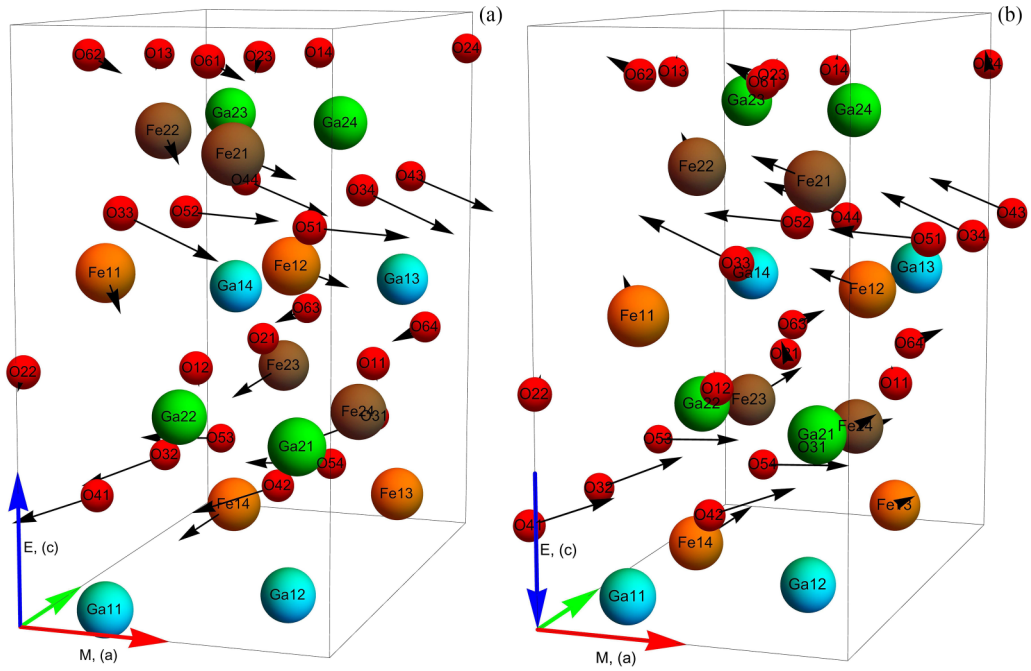

FIG. 1. (a) Unit cell in the $P_z > 0$ polarization state. The black arrows show displacements of atoms changing state $P_z > 0$ to the (b) state with $P_z < 0$. The black arrows in (b) show displacements of atoms changing state $P_z < 0$ to the (a) state $P_z > 0$. The view direction is chosen in a way that the largest displacements are clearly shown. The colored arrows in the axes' origin show directions of magnetization (red, *a*), electrical polarization (blue, *c*), and the third, orthogonal direction (green, *b*). Fe atoms at site 1 related to $Pna2_1$ symmetries (x, y, z), $(x + 1/2, -y + 1/2, z)$, $(-x, -y, z + 1/2)$, and $(-x + 1/2, y + 1/2, z + 1/2)$ are abbreviated by Fe11, Fe12, Fe13, and Fe14, respectively. The same rule applies to atoms in other sites.

Up to now, the experimental switching between two polarizations states was only observed in polycrystalline $GaFeO_3$ [13], in Ga-Fe-O thin films grown by pulsed laser deposition [14–17], and on Ga-Fe-O thin films doped by Mg [18], In [19], Cr [20], or Sc [21].

In this paper, we propose an explanation of apparent inconsistency among experimentally observed switching between two polarization states in disordered $GaFeO_3$ crystals and a theoretical description [10] valid only for fully ordered crystals. We provide proof of the electrical polarization switching on a single crystal by piezoresponse atomic force microscopy (PFM). Moreover, we provide electronic structure calculations, particularly the energies related to the disorder's effect. Finally, we compare calculations with the Mössbauer spectroscopy (MS) measurements, providing a consistent description of microscopic $GaFeO_3$ properties.

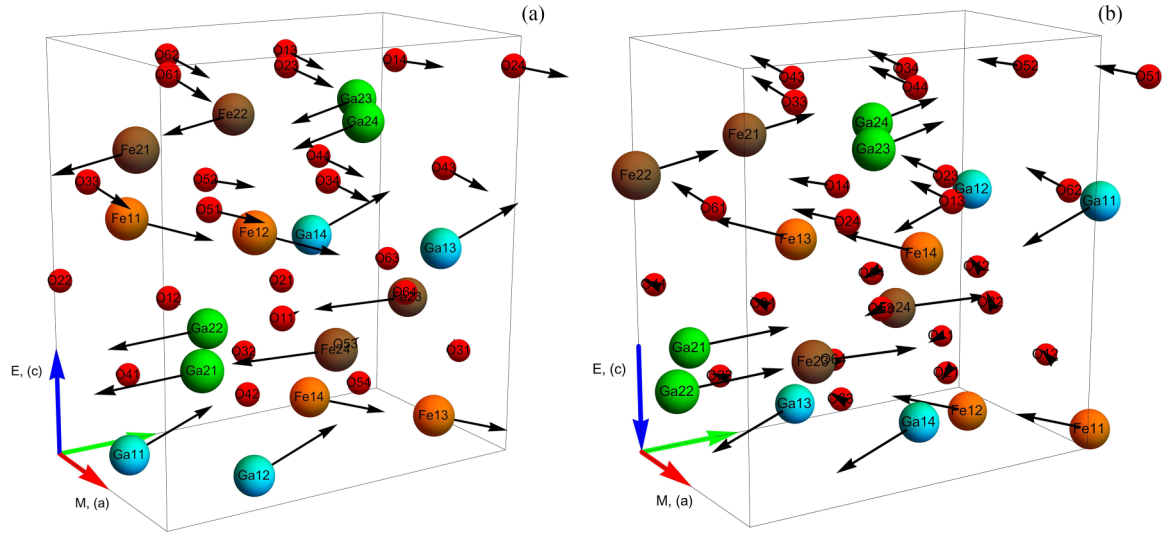

FIG. 2. Schematic view of the proposed switching between two polarization states (a), (b) (the description is the same as in the caption of Fig. 1). The structure shown in (b) was obtained by inversion of (a) and by a shift $s = (0,\ 0.249,\ 0.583)$.

TABLE I. Crystal growth direction misorientation and cation site occupations obtained by single-crystal diffraction for the single crystals used in MS and PFM experiments.

Site	Site composition Fe/Ga	Site composition Fe/Ga
	Grown in *a* direction (2°–4° misorient., used in MS)	
Fe1	0.724(7)/0.276(7)	0.747(6)/0.253(6)
Fe2	0.736(8)/0.264(8)	0.762(7)/0.238(7)
Ga1	0.081(14)/0.929(14)	0/1 Assumed
Ga2	0.477(10)/0.523(10)	0.480(10)/0.520(10)
	Grown in *c* direction (12° misorient., used in MS)	
Fe1	0.724(7)/0.276(7)	0.747(6)/0.253(6)
Fe2	0.736(8)/0.264(8)	0.762(7)/0.238(7)
Ga1	0.074(14)/0.936(14)	0/1 Assumed
Ga2	0.479(10)/0.521(10)	0.483(10)/0.517(10)
	Grown in *a* direction (5° misorient., used in PFM)	
Fe1	0.745(8)/0.255(8)	0.762(7)/0.238(7)
Fe2	0.733(8)/0.267(8)	0.748(6)/0.252(6)
Ga1	0.057(14)/0.953(14)	0/1 Assumed
Ga2	0.481(10)/0.519(10)	0.483(10)/0.517(10)

II. SINGLE-CRYSTAL GROWTH AND ORIENTATION

The $GaFeO_3$ single crystals were grown by the optical floating zone crystal growth technique according to [1,12], with a four-mirror optical floating zone furnace (FZ-T-4000-H, Crystal Systems Corp., Japan). The starting materials were powders of Fe_2O_3 (99.999%, Acros Organics) and Ga_2O_3 (99.99%, Sigma-Aldrich) in stoichiometric amounts. The growth was performed in pure oxygen under pressure between 9.0–9.2 bars and 0.4 l/min flow rate. Crystals were grown at the rate of 3–5 mm/h, with feed and seed rods rotated at 15 rpm in the opposite directions. The growth direction was enforced using oriented $GaFeO_3$ seeds in the *a* or *c* crystallographic direction [22,23]. The misorientation of growth directions with respect to the crystalline directions is listed in Table I.

The crystal orientation was performed using pieces of about 300 μm for which x-ray diffraction data were collected at room temperature. The Rigaku SuperNova diffractometer using Mo $K\alpha$ radiation ($\lambda = 0.710\,73$ Å) was used. Diffraction data were evaluated with the CRYSALISPRO package [24]. The crystal structures were solved using direct methods with SHELXT [25] and refined with SHELXL [25] using the independent atom model. The $GaFeO_3$ site occupancy was calculated assuming perfect crystal stoichiometry. The results are presented in Table I.

III. MICROSCOPIC POLARITY SWITCHING MECHANISM

An example of atomic displacements resulting in a polarization switch between two states, $P_z < 0$ and $P_z > 0$, within the $GaFeO_3$ unit cell is shown in Fig. 2. These shifts maintain the local atomic environments; i.e., the local environment of Fe1 in a state with $P_z > 0$ is changing to the same local environment in a state with $P_z < 0$. The inversion symmetry applied to the unit cell depicted in Fig. 1(a) results in the $P_z < 0$ configuration (see Table II, columns 6–8). Figure 2(b) illustrates this structure, which has been displaced by the vector $s = (0,\ 0.249,\ 0.583)$. In this shifted configuration, the distances between corresponding pairs of atoms [i.e., those with shifts indicated by antiparallel arrows in Figs. 2(a) and 2(b)] within unit cells of $P_z > 0$ and $P_z < 0$ are minimized. The upper limit of the distance between the paired atoms, denoted as $D(s)$, is equivalent to the length of the longest arrow shown in Figs. 2(a) and 2(b). The formal definition of $D(s)$ is provided in the Supplemental Material [26].

For a comprehensive list of paired atoms, please refer to Table S1 in the Supplemental Material [26]. A detailed description of the algorithm utilized for determining $D(s)$ and establishing atom pairing is presented in the Supplemental Material [26]. The previously mentioned displacement, represented as $s = (0,\ s_y,\ s_z) = (0,\ 0.249,\ 0.583)$, corresponds to the minimum value of $D(s)$. In accordance with the expected crystal symmetry, the shifts $(1,\ s_y,\ s_z)$, $(0,\ 1 - s_y,\ s_z)$, and $(1,\ 1 - s_y,\ s_z)$ also correspond to local minima of $D(s)$ with identical depths, as confirmed through numerical calculations. In periodic systems, the shifts $(0,\ s_y,\ s_z)$ and $(1,\ s_y,\ s_z)$ are considered equivalent, but we have included both for clarity, as they specify the positions of the four local minima within the unit cell. Additionally, it was found that there are another four inequivalent minima of $D(s)$ corresponding to the shifts $(0,\ s_y,\ s_z)$, $(1,\ s_y,\ s_z)$, $(0,\ 1 - s_y,\ s_z)$, and $(1,\ 1 - s_y,\ s_z)$, where $s_y = 0.263$ and $s_z = 0.076$. These minima are slightly less profound and correspond to a maximum displacement of cations larger by 0.36% and anions smaller by 3.4%; see Table S2 in the Supplemental Material [26].

In the proposed switching, the maximal distance followed by cations is 2.3 Å. It is larger than the maximal shift of oxygen anions of 1.2 Å [10]. Nevertheless, the requirement of the same atomic order of both polarization states is fully preserved in the proposed approach.

We have calculated spontaneous polarization as a multivalued vector quantity using point-charge approximation and the modern theory of polarization [27]. We get identical values

TABLE II. The atomic coordinates for specific polarization states of $GaFeO_3$. Columns 2–4: $P_z > 0$ state in asymmetric unit; columns 6–8: $P_z < 0$ state in asymmetric unit, obtained by inversion; columns 9–11: $P_z < 0$ state shifted by vector $s = (0,\ 0.249,\ 0.583)$. The coordinates located outside of the unit cell ($P_z < 0$ state) are shifted by Bravais lattice translations. $a = 5.0853$ Å, $b = 8.7451$ Å, $c = 9.3902$ Å.

$P_z > 0$	x	y	z	$P_z < 0$	x	y	z	x	y	z
1	2	3	4	5	6	7	8	9	10	11
Fe11	0.1893	0.1525	0.5827	Fe13	0.1893	0.1525	0.9173	0.1893	0.4018	0.5000
Fe21	0.6787	0.0351	0.7992	Fe22	0.8213	0.5351	0.2008	0.8213	−0.2156	0.7835
Ga11	0.1761	0.1501	0.0000	Ga13	0.1761	0.1501	0.5000	0.1761	0.3994	0.0827
Ga21	0.8091	0.1597	0.3067	Ga22	0.6909	0.6597	0.6933	0.6909	−0.0910	0.2760
O11	0.9740	0.3223	0.4260	O53	0.8410	0.1715	0.8286	0.8410	0.4208	0.4113
O21	0.5168	0.4877	0.4313	O54	0.3410	0.3285	0.8286	0.3410	0.5778	0.4113
O31	0.6521	0.9963	0.2008	O12	0.5260	0.8223	0.5740	0.5260	1.0716	0.1567
O41	0.1475	0.1593	0.1961	O22	0.9832	0.9877	0.5687	−0.0168	0.2370	0.1514
O51	0.8410	0.1715	0.6714	O24	0.0168	0.0123	0.0687	1.0168	0.2616	0.6514
O61	0.5153	0.1725	0.9379	O33	0.6521	0.9963	0.2992	0.6521	0.2456	0.8819

as for the switching proposed in the literature [10]. This is an expected result as the electric polarization can be determined in the Berry phase approach by following a path connecting the polar structure to a centrosymmetric structure, and the choice of the transition path has no impact on the result itself.

IV. DETAILS OF *AB INITIO* CALCULATIONS

The first-principles calculations were performed using the projector augmented wave (PAW) potentials [28] and the generalized gradient approximation (GGA) in the Perdew, Burke, and Ernzerhof (PBE) parametrization [29]. We have used the VASP code [30–32], and the calculations were based on the stoichiometric $GaFeO_3$. We included three valence electrons for Ga atoms ($4s^2\ 4p^1$), eight for Fe atoms ($3d^7\ 4s^1$), and six for O atoms ($2s^2\ 2p^4$). The Hubbard parameter U and exchange interaction J were optimized for the ion's magnetic moment to fit with the experiment ($U = 8$ eV, $J = 1$ eV) [1,33,34]. A plane-wave energy cutoff of 520 eV was used. The conjugate gradient algorithm was used to optimize the structure with the energy convergence criteria set at 10^{-8} and 10^{-6} eV for electronic and ionic iterations, respectively. For the summation over the reciprocal space, we used a $10 \times 6 \times 6$ Monkhorst-Pack k-point grid [35]. The simulations were performed for the orthorhombic unit cell, consisting of eight formula units (40 atoms). The electric field gradient (EFG) tensors at the positions of the atomic nuclei are calculated using the method described in the literature [36,37]. The results are presented in Table III.

The first-principles calculations show evident change of the EFG when a Fe impurity enters into Ga sites. This effect could not be obtained in point-charge calculations performed earlier [8,9]. Moreover, the quadrupole splitting (QS) of Ga1 is very close to that of Fe1 (compare QS in columns 2 and 4, 6 and 8, and 10 and 12 in Table IV). This may be the reason why only three well-resolved components were detected in Mössbauer experiments reported so far.

V. RESULTS OF ATOMIC DISORDER ENERGY CALCULATIONS

To determine which positions are energetically favorable for additional Fe atoms, we have calculated the crystal energy when one Ga atom is substituted by a Fe atom in the unit cell. The calculations were done for two nonequivalent Ga sites, resulting in the off-stoichiometric crystal $Ga_{2-x}Fe_xO_3$ with $x = 1.125$; see Table V. The additional Fe atom prefers to occupy the Ga2 site (with the magnetic moment direction at the additional Fe atom in the direction opposite that of the moment at Fe1 atoms). On the other hand, the case of one Fe atom substituted by a Ga atom in two nonequivalent Fe sites ($Ga_{2-x}Fe_xO_3$ with $x = 0.875$) leads to similar energies. Thus, both additional Fe atom positions are almost equally probable, while additional Ga goes to either the Fe1 or Fe2 site; see Table V. Note that the solution with the lowest energy for the Fe atom in the Ga1 position exhibits a magnetic moment direction identical to that of the Fe1 atoms (its energy indicated in the first row of Table V). The alteration of the magnetic moment at the additional Fe atom in the Ga site results in an increase in the total energy by 0.115 and 0.063 eV for Fe in the Ga1 and Ga2 positions, respectively.

We also investigated the effect of atomic disorder in the form of an interchange between Fe and Ga sites, as shown in Table VI. For example, for a given Fe1 position, there are four positions of Ga1 in the unit cell, corresponding to four symmetry operations of the $Pna2_1$ structure, abbreviated by Ga11, Ga12, Ga13, and Ga14, respectively.

Let us underline that all calculations presented in this section were performed for structures (atom locations) as in the optimized cell of the ideal crystal. We have also checked that optimization of the atomic positions of the structures collected in Table V leads to the decrease of the total energies of the system by 0.008, 0.005, 0.015, and 0.013 eV (respectively, from the top of Table V). Thus, the approximation employed, which utilizes atom positions similar to those in an ideal crystal, appears to be reliable, as the differences observed in Table VI relative to the ideal crystal are at least ten times larger, approximately.

VI. MÖSSBAUER EXPERIMENTS

Details of the Mössbauer experiment are given in [23]. The single crystals grown in the a and in c directions (Table I) were used for the preparation of single-crystalline, oriented absorbers. The measurements were performed at

TABLE III. Theoretical values of the EFG tensor components V_{ij} of ^{57}Fe probe at cationic sites of $GaFeO_3$. Symbol V_{kk} is the dominant component of the EFG tensor in the local principal axes system $\boldsymbol{e}_i$, $\boldsymbol{e}_j$, $\boldsymbol{e}_k$, where their Cartesian components in the unit cell frame $\boldsymbol{x}$, $\boldsymbol{y}$, $\boldsymbol{z}$, are listed in columns 4–12; indices i, j, k are ordered so that $|V_{ii}| \leqslant |V_{jj}| \leqslant |V_{kk}|$. The asymmetry parameter (column 3) is defined as $\eta = (V_{ii} - V_{jj})/V_{kk}$.

			$\boldsymbol{e}_i$			$\boldsymbol{e}_j$			$\boldsymbol{e}_k$		
	V_{kk} (V/Å^2)	η	$\boldsymbol{e}_i \cdot \boldsymbol{x}$	$\boldsymbol{e}_i \cdot \boldsymbol{y}$	$\boldsymbol{e}_i \cdot \boldsymbol{z}$	$\boldsymbol{e}_j \cdot \boldsymbol{x}$	$\boldsymbol{e}_j \cdot \boldsymbol{y}$	$\boldsymbol{e}_j \cdot \boldsymbol{z}$	$\boldsymbol{e}_k \cdot \boldsymbol{x}$	$\boldsymbol{e}_k \cdot \boldsymbol{y}$	$\boldsymbol{e}_k \cdot \boldsymbol{z}$
1	2	3	4	5	6	7	8	9	10	11	12
Fe11	−31.989	0.627	0.768	−0.516	−0.379	−0.075	0.516	−0.853	0.636	0.684	0.358
Fe21	34.138	0.995	−0.287	0.172	0.942	0.956	0.113	0.271	−0.060	0.978	−0.198
Ga11	−30.032	0.413	−0.395	0.811	0.432	0.253	−0.356	0.900	0.883	0.464	−0.064
Ga21	−56.012	0.460	0.825	−0.554	0.112	0.353	0.350	−0.868	0.442	0.756	0.484
Ga11[a]	−32.885	0.178	−0.457	0.773	0.440	0.262	−0.356	0.897	0.850	0.525	−0.040
Ga21[a]	−71.963	0.485	0.822	−0.556	0.121	0.359	0.342	−0.868	0.442	0.757	0.481

[a]Results of calculations for single iron at the foreign site of $GaFeO_3$.

room temperature. Using electronic structure calculations on ideal $GaFeO_3$ and on single Fe cations at Ga sites, we obtained electric field gradients on the ^{57}Fe probe at cationic sites (Table III). With the help of the full Hamiltonian formalism [38] adapted to the $GaFeO_3$ crystal [23], we have calculated parameters of doublets for the ^{57}Fe iron probe at different sites and orientations of the k vector (Table IV).

The experimental spectra of $GaFeO_3$ consist of overlapping subspectra, and the assignment of absorption lines to the sites is not apparent. Also, the ambiguity problem is present, i.e., the continuous distribution of parameters results in the exact shape of the spectrum. The measurements of texture-free absorbers in external magnetic fields were performed to make the interpretation precise. Moreover, the measurements of single-crystal absorbers with the orientation of the wave vector k parallel to the main crystal directions were done. One of the most difficult problems is spectra interpretation; the orientation of the EFG was solved by adopting principal directions obtained by electronic structure calculations. Also, the asymmetry parameter in the in-magnetic field experiment was adopted from the theoretical calculations. It is worthwhile to add that throughout the paper, we use four colors related to the four cationic sites, already shown on unit cells (Figs. 1 and 2) and also used for the abbreviation of the subspectra in Figs. 3 and 4 or sites in Figs. 7 and 8.

The results of single-crystal measurements, with the k vector parallel to the three main crystallographic directions, are presented in Fig. 3. Relative line intensities in the doublets were taken from theoretical calculations [38] (Table IV, A_1/A_2). The results from the powdered single crystals are shown in Fig. 4. In order to avoid the problem with the crystal texture, the measurements with a so-called magic angle were done [39]. The measured spectrum [see Fig. 4(a)] is a superposition of a few not well-resolved doublets from the iron atoms in the $GaFeO_3$ structure. In order to get more data, the measurements in an external magnetic field of $B = 1$ and 1.3 T, parallel to the beam direction, were conducted. In the analysis of in-field measurements, the Blaes procedure was used [40]. The hyperfine fields induced in the local position in the $GaFeO_3$ were free parameters in the fitting. The simultaneous fit shows that three subspectra are needed to describe the shapes of measured spectra well. The solid red line represents the best fit, while the other lines represent three subspectra. The hyperfine parameters and relative intensities of the doublets are presented in Table VII. The analysis shows that Fe atoms occupy only three octahedral positions in the crystal structure of $GaFeO_3$. Almost the same fraction of iron occupies the Fe1 and Fe2 sites, while in the Ga2 sites, the fraction of iron is twice as small as in the Fe1 and Fe2 sites. There is no experimental evidence within the limits of

TABLE IV. Theoretical values of the parameters of the Mössbauer spectra. QS $= \frac{eQcV_{zz}}{2E_0}\sqrt{1+\eta^2/3}$ – separation between two absorption lines in the quadrupole doublet; A_1/A_2: a ratio of the absorption line intensities in the doublet, k: direction of the wave vector of a photon with respect to the main crystal direction (reference of $Pna2_1$ space group). Symbol e is the elementary charge, Q is the nuclear quadrupole moment of the first excited state of ^{57}Fe (1.7×10^{-29} m^2), E_0 is the energy of a photon in Mössbauer excitation (14.412 497 keV); c: is the speed of light.

k	100	100	100	100	010	010	010	010	001	001	001	001
Site	Fe1	Fe2	Ga1	Ga2	Fe1	Fe2	Ga1	Ga2	Fe1	Fe2	Ga1	Ga2
1	2	3	4	5	6	7	8	9	10	11	12	13
QS	−0.30	0.35	−0.29	−0.66	−0.30	0.35	−0.29	−0.66	−0.30	0.35	−0.29	−0.66
A_1/A_2	1.31	2.3	1.84	0.93	1.21	0.42	0.96	1.49	0.62	1.03	0.57	0.72
Site	Fe1	Fe2	Ga1[a]	Ga2[a]	Fe1	Fe2	Ga1[a]	Ga2[a]	Fe1	Fe2	Ga1[a]	Ga2[a]
QS	−0.3	0.35	−0.27	−0.51	−0.3	0.35	−0.27	−0.51	−0.3	0.35	−0.27	−0.51
A_1/A_2	1.31	2.3	2.01	0.93	1.21	0.42	0.94	1.48	0.62	1.03	0.54	0.73

[a]Results of calculations for single iron at the foreign site of $GaFeO_3$.

TABLE V. Energies of nonstoichiometric $Ga_{2-x}Fe_xO_3$ crystal with a different type of disorder. In the unit cell composed of 40 atoms, one Fe atom was substituted by one Ga atom, or one Ga atom was substituted by one Fe atom. The energy of the ideal crystal is $E_0 = -250.6123346$ eV.

	x	Site disorder	Energy (eV)
1.	1.125	Fe in Ga1	−251.6327450
2.	1.125	Fe in Ga2	−251.8857439
3.	0.875	Ga in Fe1	−249.2106457
4.	0.875	Ga in Fe2	−249.2295923

experimental uncertainty that Fe is located in the tetrahedral Ga sites.

VII. PIEZORESPONSE FORCE MICROSCOPY

Piezoresponse force microscopy (PFM) is designed to measure piezoelectric and ferroelectric materials on the nanoscale [41]. All measurements used a NanoWizard 3 BioScience (JPK Instruments, Berlin, Germany) atomic force microscope (AFM). Images were acquired at room temperature using conductive diamond-coated AFM tips with resonant frequencies close to 110 kHz. The experimental setup allowed tip/detector calibration to measure PFM response in picometers. The modulation voltage was set to 1 V, which gave a relatively strong PFM signal. In addition, the bias voltage was applied in the range of 0–20 V, depending on the experiment. The piezoswitching (images) were obtained with no bias, where the polarization change was forced by +5 V bias, while the PFM spectroscopy was performed in the range of ±20 V. The data analysis was performed using GWYDDION software [42].

TABLE VI. The energy of site disorder. A pair of Fe and Ga atoms (column 2) interchange their positions in the unit cell resulting in energy listed in column 3. Values averaged over sites generated by symmetry operations are listed in column 4.

1	Interchange of two atoms between sites 2	Energy E (eV) 3	$\bar{E} - E_0$ (eV) 4
1.	Fe11, Ga11	−250.2321563	
2.	Fe11, Ga12	−250.2413128	0.378
3.	Fe11, Ga13	−250.2316511	
4.	Fe11, Ga14	−250.2329995	
5.	Fe11, Ga21	−250.4597895	
6.	Fe11, Ga22	−250.4776731	0.143
7.	Fe11, Ga23	−250.4564648	
8.	Fe11, Ga24	−250.4833769	
9.	Fe21, Ga11	−250.2065841	
10.	Fe21, Ga12	−250.2365022	0.384
11.	Fe21, Ga13	−250.2498087	
12.	Fe21, Ga14	−250.2225650	
13.	Fe21, Ga21	−250.5050056	
14.	Fe21, Ga22	−250.5045072	0.112
15.	Fe21, Ga23	−250.4888525	
16.	Fe21, Ga24	−250.5055941	

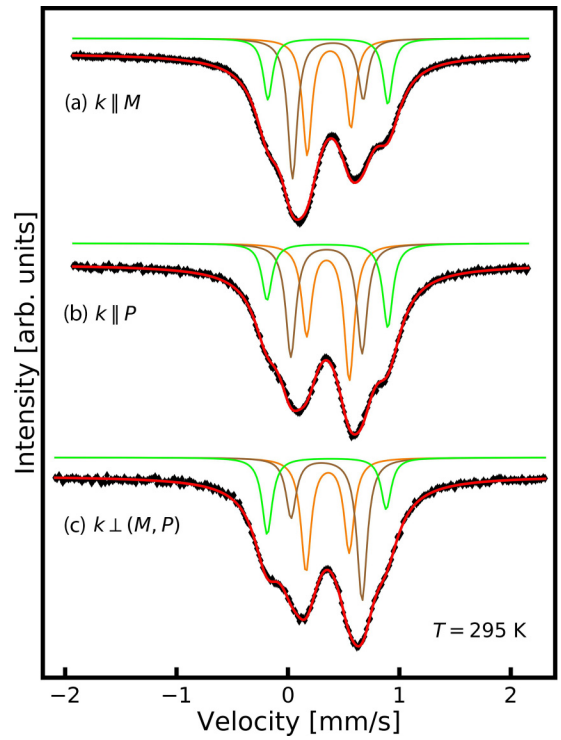

FIG. 3. Mössbauer spectra of single crystals measured with the k vector parallel to the three main crystallographic directions. Relative line intensities in the doublets are taken from theoretical calculations (Table III), while other parameters are listed in Table IV. Colored curves represent subspectra of iron located in Fe1 (orange), Fe2 (brown), and Ga2 (green) sites. The red curve is a fit to experimental data (black points).

The sample plane of dimensions 3.9 mm × 3.9 mm was cut from a single crystal grown along the a axis ($Pna2_1$ space group). The plane was perpendicular to the c crystallographic axis within an accuracy of 2°. By intensive PFM investigations, we could not find a visible ferroelectric domain structure registered down to the nanoscale range. It suggests that the sample was a single domain or that the domain size was above the maximum possible scan size of the implemented AFM equipment, which was 100 μm × 100 μm. However, to the best of our knowledge, reports of such ferroelectric domains (on single crystals) using other techniques like surface decoration, etching, optical microscopy, polarized light microscopy, x-ray techniques, or electron microscopy techniques are rare. It is consistent with the fact that relatively large energy is needed to switch between opposite polarizations, as mentioned previously.

Nevertheless, the piezoresponse signal from the sample was relatively strong, showing typical piezoelectric behavior. First, a number of scans of the same regions were performed. We have started by scanning the region of 7.5 μm × 7.5 μm with +5 V bias, followed by a 5 μm × 5 μm with −5 V bias, and finished by 2.5 μm × 2.5 μm again with +5 V bias. Next, we measured the same region in a larger scan of 10 μm × 10 μm with no extra bias voltage. The result is shown in Figs. 5(a) and 5(b) where the PFM amplitude and phase are presented. The images are a pseudo-three-dimensional (3D) maps, where the value is correlated with the color. Thus the

TABLE VII. Parameters of hyperfine interactions for subspectra are shown in Figs. 3 and 4. The asymmetry parameter η was adopted from theoretical calculations (Table III). Sub1, Sub2, and Sub3 are spectral areas proportional to the number of Fe atoms in the site; Sub4 = 0 was assumed since this spectral area was below a detection limit. ISO is the isomer shift measured relative to α-iron at room temperature, QS is the quadrupole splitting between nuclear excited and ground states, BHF is the hyperfine magnetic field, and ARE is the fraction of the area under the spectrum.

	ISO ± 0.02 [mm/s]			QS ± 0.02 [mm/s]			BHF ± 0.07 [T]			ARE ± 2[%]		
Sample	Sub1	Sub2	Sub3	Sub1	Sub2	Sub3	Sub1	Sub2	Sub3	Sub1	Sub2	Sub3
Single crystal	0.36	0.35	0.36	−0.39	0.64	−1.08	–	–	–	38	38	24
Powder, magic angle	0.37	0.36	0.36	−0.39	0.64	−1.08	–	–	–	38	38	24
Powder, $B_{ext} = 1$ T	0.35	0.35	0.34	−0.36	0.62	−1.05	1.16	0.89	0.53	38	38	24
Powder, $B_{ext} = 1.3$ T	0.36	0.35	0.35	−0.40	0.68	−1.10	1.22	0.95	0.59	38	38	24

higher the color, the higher the value. One can see that it is possible to control the polarization of the $GaFeO_3$ single crystal. Namely, it is possible to switch crystal polarization along a certain direction by a specific voltage. For more detail, a profile along the white line was extracted for both the PFM amplitude and phase, shown in Figs. 5(c) and 5(d). However, one has to keep in mind that the voltage applied to the conducting AFM tip produces relatively high electric fields. In our case, the electric field applied in the PFM technique was in the range of at least 500 kV/cm^{-1} (5 V over a distance of 100 nm, which is a very conservative estimation of the tip-surface distance).

Second, PFM spectroscopy in a single point was performed in the range of ±20 V. The typical results are shown in Fig. 6. The PFM amplitude and phase contrast are shown as a function of bias voltage. The switching between the two polarization states is visible, with the coercive voltage close to 2 V. The presented data are a result of subsequent switching of the same point and are representative for the whole sample. The phase change [Fig. 6(b)] also shows the change in the polarization state of 180°, further confirming that the switching occurred between two opposite polarization states.

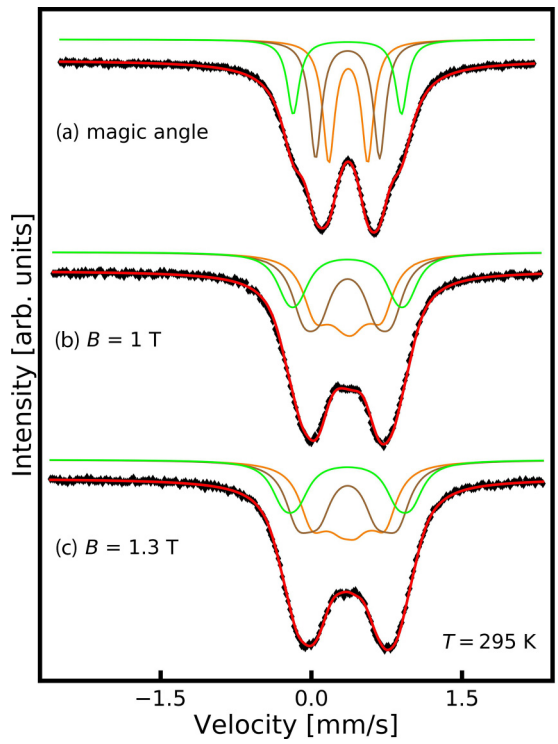

FIG. 4. Mössbauer spectra of powdered single crystals measured at a magic angle (a) and in external magnetic fields (b), (c). Relative line intensities in the doublets are taken from theoretical calculations (Table III). The description of colored curves is the same as in Fig. 3.

VIII. DISCUSSION

The results of theoretical calculations of the electric field gradient tensor allow the use of its local orientations in data analysis. The relative line intensities in the doublets of Mössbauer spectra shown in Fig. 3 were calculated without the use of any fitting procedure. Also, the predicted asymmetry parameter (Table III) was used in the data analysis of spectra measured in an external magnetic field (Fig. 4). These theoretical predictions agree perfectly with the experimental observations (Fig. 3).

The values of isomer shifts ranging between 0.35 and 0.37 mm/s in $GaFeO_3$ are typical for the oxidation state of iron 3^+ in the high spin state [43]. The experimental values of the quadrupole splitting, Fe1: −0.39(2); Fe2: +0.64(2); Ga2: −1.08(2) (in mm/s, Table VII) correlates reasonably well with the results of electronic structure calculations, Fe1: −0.30; Fe2: +0.35; Ga1: −0.29; Ga2: −0.66 (in mm/s, Table IV); in particular, the signs of the EFG fully agree. In order to investigate the effect of the lattice contribution to EFG, the point-charge calculations were performed and it was found that the results fully agree with the earlier reported values [9]. The absolute values of V_{zz}, Fe:+1.18; Fe2: +1.36; Ga1: −1.31; Ga2: −2.42 (in V/Å^2) are nicely correlated with the theoretical calculations (Table III, column 1), although the sign of EFG of Fe1 in point-charge calculations does not agree with the theoretical calculation as well as the experimental value. These facts show that there is a large contribution of the lattice to the EFG although it does not fully explain the experimentally observed values. The spin-orbit interaction for the d^5 electron configuration subject to a ligand field of octahedral symmetry is typically small [44]; however, in the case of distorted octahedra it may be nonzero [33] and may influence the EFG.

The atomic disorder measured by x-ray diffraction (Table I) is consistent with that determined in Mössbauer experiments (Table VIII). It plays a crucial role in our investigations, as it allows the estimation of the atoms'

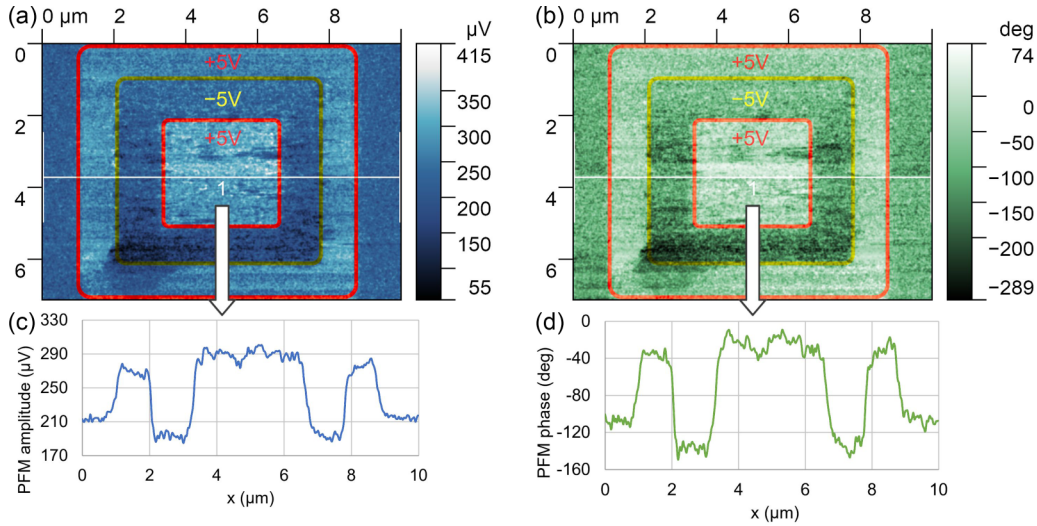

FIG. 5. PFM images of oriented $GaFeO_3$ single crystal showing (a) PFM amplitude and (b) PFM phase-contrast images acquired over a 10 µm × 7.5 µm area, followed by the profiles of (c) PFM amplitude and (d) PFM phase, extracted along the white line on the images. The images are a result of a sequence of previous scans of the central region: 7.5 µm × 7.5 µm area with +5 V bias, 5 µm × 5 µm area with −5 V bias, and 2.5 µm × 2.5 µm area with +5 V bias. This led to switching the piezoelectric polarization of the region.

energies entering the foreign sites. It can also serve as the evaluation for the model predicting the electrical switching polarization.

It is clear from Table V (rows 1,2) that Fe in the Ga1 site has larger energy than in the Ga2 site by about 0.257 eV. This value coincides nicely with energies of interchange presented in Table V for defect creation of Fe in the Ga1 position. This energy is 0.384 and 0.378 eV on average: Fe2 in Ga1 is slightly larger than Fe1 in Ga1. The calculations also show that the energies of the Ga location in foreign sites Fe1 and Fe2 are very similar. In crystals with an excess of gallium $x = 0.875$ (Table V, rows 3,4), Ga in the Fe1 site has larger energy than in the Fe2 site by 0.025 eV. Analysis of pair interchange in stoichiometric crystal shows a similar effect; the interchange of Fe1 and Ga2 atoms requires energy larger by about 0.031 eV than that of Fe2 and Ga2. One expects Ga in both the Fe2 and Fe2 sites to locate easily, while Fe should hardly enter the Ga1 sites.

The results of theoretical calculations are consistent with a simple model of structural defects. Let us simplify interactions by assuming that, on average, Fe or Ga atoms entering the foreign site increase the crystal energy by a value independent of their geometrical arrangement in the unit cell. This assumption is governed by the observation in Table VI that in rows 1–4, the energies are similar to each other, and in rows 5–8, 9–12, and 13–16 as well. We also neglect the compositional dependence of the energies in the range covered in Table V. We thus introduce energy $E_{\mathrm{Fe}}^{(1)}$ corresponding to the presence of foreign Fe in the Ga1 site. Further energies are defined consequently: $E_{\mathrm{Fe}}^{(2)}$, $E_{\mathrm{Ga}}^{(1)}$, and $E_{\mathrm{Ga}}^{(2)}$. We may write for the third

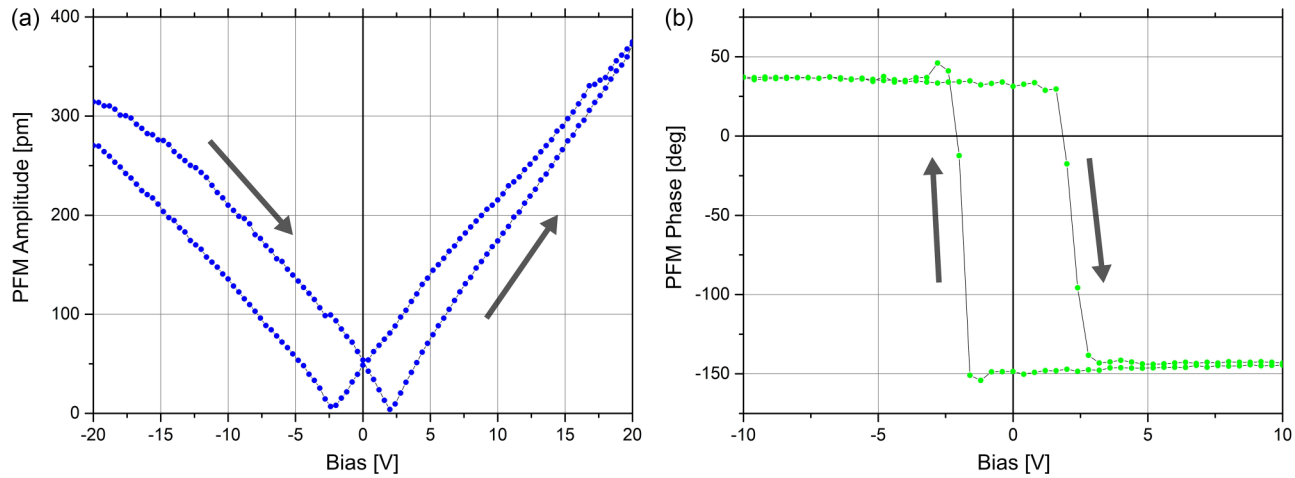

FIG. 6. PFM spectroscopy curves of oriented $GaFeO_3$ single crystal showing (a) amplitude and (b) phase-change signals as a function of bias voltage performed at a random sample position. The results show switching between two piezoelectric polarization states. Arrows point in the direction of the voltage sweep, the up arrow is from +10 to −10 V, while the down arrow is the opposite.

TABLE VIII. Site composition derived from the Mössbauer experiment and occupation numbers defined as fractions of foreign atoms. The site compositions (column 2) are proportional to the ARE presented in Table VII, columns Sub1, Sub2, Sub3: $2 \times (37.0,\ 40.7,\ 22.3)/100 = (0.740,\ 0.814,\ 0.446)$. Structure $P_z < 0$ is derived with assumptions of the model presented in [10].

Site	Site composition Fe/Ga	Occupation numbers
Structure $P_z > 0$		
Fe1	0.740/0.260	$c_{1\mathrm{Ga}} = 0.26(1)$
Fe2	0.814/0.186	$c_{2\mathrm{Ga}} = 0.19(4)$
Ga1	0.000/1.000	$c_{1\mathrm{Fe}} = 0.00(4)$
Ga2	0.446/0.554	$c_{2\mathrm{Fe}} = 0.45(1)$
Structure $P_z < 0$		
Fe1	0.814/0.186	$c_1 = 0.19(4)$
Fe2	0.740/0.260	$c_2 = 0.26(1)$
Ga1	0.446/0.554	$c_3 = 0.45(1)$
Ga2	0.000/1.000	$c_4 = 0.00(4)$

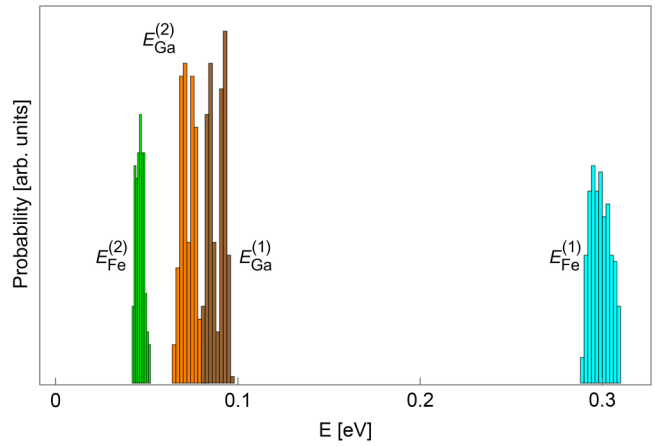

FIG. 7. Distribution of energies $E_{\mathrm{Fe}}^{(1)}$, $E_{\mathrm{Fe}}^{(2)}$, $E_{\mathrm{Ga}}^{(1)}$, and $E_{\mathrm{Ga}}^{(2)}$; see text for precise definition. One should not confuse the colors used and sites Fe1, Fe2, Ga1, and Ga2.

column of Table V,

$$E_{\mathrm{Fe}}^{(2)} - E_{\mathrm{Fe}}^{(1)} - u_2 + u_1 = 0, \tag{1}$$

$$E_{\mathrm{Ga}}^{(2)} - E_{\mathrm{Ga}}^{(1)} - u_4 + u_3 = 0, \tag{2}$$

$$E_{\mathrm{Ga}}^{(1)} + E_{\mathrm{Ga}}^{(2)} + E_{\mathrm{Fe}}^{(1)} + E_{\mathrm{Fe}}^{(2)} - 4e_0 = 0, \tag{3}$$

where u_i is given in the ith row of Table V and e_0 is the energy of an unperturbed crystal, shown in the caption of Table V. Similarly,

$$E_{\mathrm{Fe}}^{(1)} + E_{\mathrm{Ga}}^{(1)} - v_{1,4} + e_0 = 0, \tag{4}$$

$$E_{\mathrm{Fe}}^{(2)} + E_{\mathrm{Ga}}^{(1)} - v_{5,8} + e_0 = 0, \tag{5}$$

$$E_{\mathrm{Fe}}^{(1)} + E_{\mathrm{Ga}}^{(2)} - v_{9,12} + e_0 = 0, \tag{6}$$

$$E_{\mathrm{Fe}}^{(2)} + E_{\mathrm{Ga}}^{(2)} - v_{13,16} + e_0 = 0, \tag{7}$$

where $v_{i,j}$ is given by any row between i and j of Table VI. Equations (1)–(7) are mathematically contradictory. However, an approximation can be obtained if energies $E_{\mathrm{Fe}}^{(1)}$, $E_{\mathrm{Fe}}^{(2)}$, $E_{\mathrm{Ga}}^{(1)}$, and $E_{\mathrm{Ga}}^{(2)}$ are chosen so that sets (1)–(7) are fulfilled approximately, with possibly minor deviations. To find the energies, we minimize the sum of squares of the left-hand side of Eqs. (1)–(7) with additional physical constraints for the energies to be positive. There are $4 \times 4 \times 4 \times 4$ numbers of choices of the energies $v_{1,4}$, $v_{5,8}$, $v_{9,12}$, and $v_{13,16}$ taken from Table VI, which appear in Eqs. (4)–(7). Calculations show that for all the choices, calculated energies are distributed within a relatively narrow range of values; see the histogram in Fig. 7. The average values and standard deviations are equal to $E_{\mathrm{Fe}}^{(1)} = 0.299(5)$, $E_{\mathrm{Fe}}^{(2)} = 0.046(2)$, $E_{\mathrm{Ga}}^{(1)} = 0.088(4)$, and $E_{\mathrm{Ga}}^{(2)} = 0.073(4)$ (in eV). These values are larger than previously estimated in [45].

Using Mössbauer experiments (Table VII), occupation numbers were extracted (Table VIII). The occupation numbers $c_{1\mathrm{Ga}}$, $c_{2\mathrm{Ga}}$, $c_{1\mathrm{Fe}}$, and $c_{2\mathrm{Fe}}$ are defined as a fraction of foreign atoms occupying Fe1, Fe2, Ga1, and Ga2 sites, respectively. Note that the index in the occupation numbers shows foreign atoms located at the site indicated by the integer. All occupation numbers are between 0 and 1; the condition of stoichiometry demands that $c_{1\mathrm{Ga}} + c_{2\mathrm{Ga}} - c_{1\mathrm{Fe}} - c_{2\mathrm{Fe}} = 0$. For perfectly ordered $GaFeO_3$, all the occupation numbers are equal to zero. For the sake of clarity, we quote that the site Fe1 consists of $1 - c_{1\mathrm{Ga}}$ Fe atoms and $c_{1\mathrm{Ga}}$ foreign Ga. The occupation numbers at thermal equilibrium can be obtained using the estimated energies and statistical approach. Assuming that in N positions of the given site (say, Fe1), there are $Nc_{1\mathrm{Fe}}$ foreign Ga atoms, and the number of possible microstates is equal to the number of all different $Nc_{1\mathrm{Fe}}$-element subsets taken from the set of N elements. Thus, the number of microstates Γ for four sites with occupation numbers $c_{1\mathrm{Ga}}, c_{2\mathrm{Ga}}, c_{1\mathrm{Fe}}, c_{2\mathrm{Fe}}$ is

$$\Gamma = \binom{N}{Nc_{1\mathrm{Ga}}}\binom{N}{Nc_{2\mathrm{Ga}}}\binom{N}{Nc_{1\mathrm{Fe}}}\binom{N}{Nc_{1\mathrm{Fe}}}, \tag{8}$$

where $\binom{n}{k}$ is $n!/[k!(n-k)!]$. Using the Stirling formula for $n!$ the entropy $S = k_B \ln\Gamma$ can be obtained from (8) in the limit of large N:

$$S = k_B N \ln f(c_{1\mathrm{Ga}}) f(c_{2\mathrm{Ga}}) f(c_{1\mathrm{Fe}}) f(c_{2\mathrm{Fe}}), \tag{9}$$

where

$$f(x) = \frac{1}{x^x (1-x)^{(1-x)}}. \tag{10}$$

The energy U is equal to

$$U = N\left(E_{\mathrm{Fe}}^{(1)} c_{1\mathrm{Fe}} + E_{\mathrm{Fe}}^{(2)} c_{2\mathrm{Fe}} + E_{\mathrm{Ga}}^{(1)} c_{1\mathrm{Ga}} + E_{\mathrm{Ga}}^{(2)} c_{2\mathrm{Ga}}\right). \tag{11}$$

The number of foreign atoms has to fulfill the chemical composition of the crystal:

$$c_{1\mathrm{Ga}} + c_{2\mathrm{Ga}} - c_{1\mathrm{Fe}} - c_{2\mathrm{Fe}} = 0. \tag{12}$$

From Eqs. (11) and (12) one can calculate $c_{1\mathrm{Fe}}$ and $c_{2\mathrm{Fe}}$. In the thermodynamic equilibrium, the entropy achieves maximum value, so the derivatives of (9) over $c_{1\mathrm{Ga}}$ and $c_{2\mathrm{Ga}}$ should vanish:

$$\frac{\partial S(c_{1\mathrm{Ga}}, c_{2\mathrm{Ga}}, U)}{\partial c_{1\mathrm{Ga}}} = 0, \quad \frac{\partial S(c_{1\mathrm{Ga}}, c_{2\mathrm{Ga}}, U)}{\partial c_{2\mathrm{Ga}}} = 0. \tag{13}$$

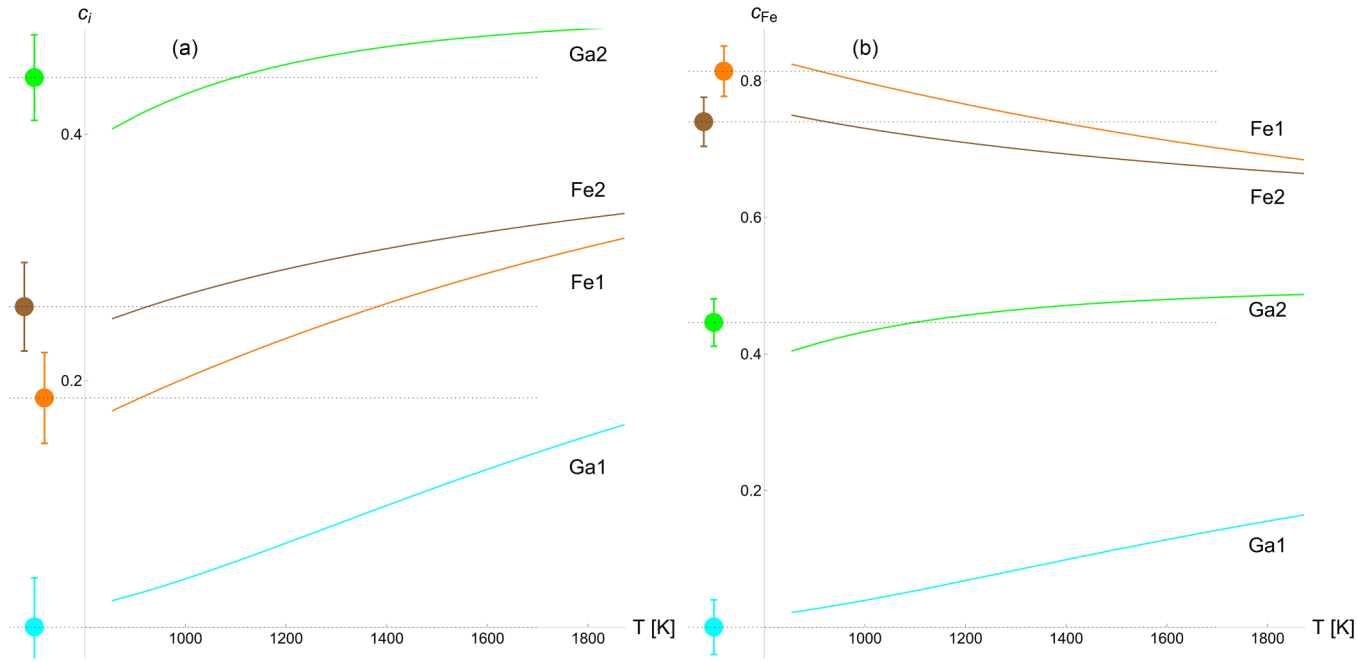

FIG. 8. (a) Foreign atom site occupancies (related to occupation numbers in the third column of Table VII) and (b) iron site occupancies. Panels (a), (b) show, in fact, the same data. The lines show predictions of thermal equilibrium site occupancies, while points on the left of each panel show results obtained from Mössbauer experiments. Experimental values do not correspond to the thermal equilibrium state.

Equation (13) allow us to find entropy as a function $c_{1\mathrm{Ga}}$, $c_{1\mathrm{Ga}}$ at given energy U. Further on, since $T = \partial U/\partial S$, one can find all the occupation numbers numerically, $c_{1\mathrm{Ga}}, c_{2\mathrm{Ga}}, c_{1\mathrm{Fe}}, c_{2\mathrm{Fe}}$, as a function of equilibrium temperature, shown in Fig. 8(a) and, more conveniently, Fe occupation of four sites of $GaFeO_3$ [see Fig. 8(b)].

Using the estimated energies of atoms in foreign sites—$E_{\mathrm{Fe}}^{(1)}$, $E_{\mathrm{Fe}}^{(2)}$, $E_{\mathrm{Ga}}^{(1)}$, and $E_{\mathrm{Ga}}^{(2)}$—in conjunction with the fractions of atoms at foreign sites as provided in Table VIII and model presented in [10], we have determined that the energy associated with the asymmetric unit for $P_z > 0$ is 0.057(13) eV, while for $P_z < 0$, it amounts to 0.170 (8) eV. The difference between these values, resulting from the switch in electrical polarization, corresponds to 31(4) kJ kg^{-1} or 1.1(1) kJ mol^{-1} of atoms. These values may be compared with the heat fusion of elements such as gallium (80 kJ kg^{-1}) or lithium (3 kJ mol^{-1}) and they show that the predicted switching energy is unphysically large.

The overall agreement of the combined data analysis, based on theoretical predictions and spectra analysis, guarantees correct spectra assignment. Measurements were done on different orientations of the single crystal, at magic angle geometry and in-magnetic fields with a consistent set of parameters (Figs. 3 and 4). This also allows for the determination of spectral areas and quantitative estimation of the atomic disorder. Theoretical calculations of some atomic configuration conditions allow energy estimations related to the atomic disorder.

We have observed the switching of the polarization state by piezoresponse force microscopy. The measurements indicate symmetric, nonbiased hysteresis of the polarization switching. Thus the microscopic mechanism proposed in [10] can be questioned because the difference in the crystal energy between polarization states 31(4) kJ kg^{-1} is expected. The concept of atomic displacements in the unit cell guarantees equal energy for two polarization states for disordered $GaFeO_3$ crystals and is consistent with observed symmetric energy switching induced by PFM spectroscopy.

IX. CONCLUSIONS

We have synthesized $GaFeO_3$ single crystals. The site disorder was determined by x-ray diffraction and the Mössbauer experiments. The microscopic energies of the disorder were estimated. The location of iron in the Ge1 octahedral site is energetically unfavorable. This substitution has energy larger by about 0.2 meV than the other three possible types of substitution (Fe in Ga2, Ga in Fe1, and Ga in Fe2). Electronic structure calculations indicate that the hyperfine parameters of Fe in the Ga1 site are close to that of Fe1. This is a possible reason for observing only three distinct components in the Mössbauer experiments performed so far. Switching of electrical polarization was demonstrated by PFM spectroscopy. A mechanism of electrical polarization switching of disordered $GaFeO_3$, consistent with physical properties measured so far, was proposed. In contrast to earlier concepts [10], the proposed mechanism preserves atomic disorder in the cationic sites and guarantees symmetric hysteresis of the electrical polarization switch.

ACKNOWLEDGMENTS

This work was partially supported by the National Science Centre (Grant No. OPUS 2018/31/B/ST3/00279). K.J.K. thanks Przemysław Piekarz and Andrzej Ptok for constructive discussions and sincerely acknowledges the hospitality

of the Henryk Niewodniczański Institute of Nuclear Physics (of the Polish Academy of Sciences) in Kraków (Poland) as well as access to their computational resources. K.J.K. thanks the Polish National Agency for Academic Exchange for funding in the frame of the Bekker program (Grant No. PPN/BEK/2020/1/00184).

[1] T. Arima, D. Higashiyama, Y. Kaneko, J. P. He, T. Goto, S. Miyasaka, T. Kimura, K. Oikawa, T. Kamiyama, R. Kumai, and Y. Tokura, Structural and magnetoelectric properties of $Ga_{2-x}Fe_xO_3$ single crystals grown by a floating-zone method, Phys. Rev. B **70**, 064426 (2004).

[2] S. C. Abrahams, J. M. Reddy, and J. L. Bernstein, Crystal structure of piezoelectric ferromagnetic gallium iron oxide, J. Chem. Phys. **42**, 3957 (1965).

[3] M. Hatnean, J. Robert, M. T. Fernandez Diaz, E. Ressouche, A. Cousson, L. Pinsard-Gaudart, and S. Petit, Neutron scattering study of the magnetoelectric compound $GaFeO_3$, Eur. Phys. J. Spec. Top. **213**, 69 (2012).

[4] S. K. Mishra, R. Mittal, R. Singh, M. Zbiri, T. Hansen, and H. Schober, Phase stability of multiferroic $GaFeO_3$ up to 1368 K from *in situ* neutron diffraction, J. Appl. Phys. **113**, 174102 (2013).

[5] W. Kim, J. H. We, S. J. Kim, and C. S. Kim, Effects of cation distribution for $AFeO_3$ (A = Ga, Al), J. Appl. Phys. **101**, 09M515 (2007).

[6] K. Sharma, V. Raghavendra Reddy, D. Kothari, A. Gupta, A. Banerjee, and V. G. Sathe, Low temperature Raman and high field ^{57}Fe Mossbauer study of polycrystalline $GaFeO_3$, J. Phys.: Condens. Matter **22**, 146005 (2010).

[7] V. Raghavendra Reddy, K. Sharma, A. Gupta, and A. Banerjee, magnetic anisotropy and sub-lattice magnetization study of polycrystalline magneto-electric $Ga_{2-x}Fe_xO_3$, J. Magn. Magn. Mater. **362**, 97 (2014).

[8] S. Nakamura, S. Morimoto, T. Saito, and Y. Tsunoda, Mössbauer study on the polar ferrimagnet $GaFeO_3$, J. Phys.: Conf. Ser. **200**, 012140 (2010).

[9] S. Nakamura, Y. Kobayashi, S. Kitao, M. Seto, and A. Fuwa, Observation of multiferroicity in $GaFeO_3$ by Mössbauer spectroscopy, J. Phys.: Conf. Ser. **592**, 012122 (2014).

[10] D. Stoeffler, First principles study of the electric polarization and of its switching in the multiferroic $GaFeO_3$ system, J. Phys.: Condens. Matter **24**, 185502 (2012).

[11] C. Ederer and N. A. Spaldin, Towards a microscopic theory of toroidal moments in bulk periodic crystals, Phys. Rev. B **76**, 214404 (2007).

[12] Y. Kaneko, T. Arima, J. P. He, R. Kumai, and Y. Tokura, Magnetic and crystal structures of polar ferrimagnet $Ga_{2-x}Fe_xO_3$, J. Magn. Magn. Mater. **272–276**, 555 (2004).

[13] R. Saha, A. Shireen, S. N. Shirodkar, U. V. Waghmare, A. Sundaresan, and C. N. R. Rao, Multiferroic and magnetoelectric nature of $GaFeO_3$, $AlFeO_3$ and related oxides, Solid State Commun. **152**, 1964 (2012).

[14] S. Mukherjee, A. Roy, S. Auluck, R. Prasad, R. Gupta, and A. Garg, Room temperature nanoscale ferroelectricity in magnetoelectric $GaFeO_3$ epitaxial thin films, Phys. Rev. Lett. **111**, 087601 (2013).

[15] G. Zhong, Y. Bitla, J. Wang, X. Zhong, F. An, Y.-Y. Chin, Y. Zhang, W. Gao, Y. Zhang, A. Eshghinejad *et al.*, Tuning Fe concentration in epitaxial gallium ferrite thin films for room temperature multiferroic properties, Acta Mater. **145**, 488 (2018).

[16] S. Song, H. M. Jang, N. S. Lee, J. Y. Son, R. Gupta, A. Garg, J. Ratanapreechachai, and J. F. Scott, Ferroelectric polarization switching with a remarkably high activation energy in orthorhombic $GaFeO_3$ thin films, npg Asia Mater. **8**, e242 (2016).

[17] T. Katayama, S. Yasui, Y. Hamasaki, T. Shiraishi, A. Akama, T. Kiguchi, and M. Itoh, Ferroelectric and magnetic properties in room-temperature multiferroic $Ga_xFe_{2-x}O_3$ epitaxial thin films, Adv. Funct. Mater. **28**, 1704789 (2018).

[18] A. Thomasson, S. Cherifi, C. Lefevre, F. Roulland, B. Gautier, D. Albertini, C. Meny, and N. Viart, Room temperature multiferroicity in $Ga_{0.6}Fe_{1.4}O_3$: Mg thin films, J. Appl. Phys. **113**, 214101 (2013).

[19] C. Song, X. Yan, Q. Liu, J. X. Sui, H. S. Zhao, S. Xu, F. Yuan, and Y. Z. Long, Magnetic and ferroelectric properties of indium-doped gallium ferrite, J. Magn. Magn. Mater. **469**, 8 (2019).

[20] T. Katayama, S. Yasui, T. Osakabe, Y. Hamasaki, and M. Itoh, Ferrimagnetism and ferroelectricity in Cr-substituted $GaFeO_3$ epitaxial films, Chem. Mater. **30**, 1436 (2018).

[21] H. Wang *et al.*, Large polarization switching and high-temperature magnetoelectric coupling in multiferroic $GaFeO_3$ systems, Inorg. Chem. **60**, 225 (2021).

[22] M. Biernacka, M. Szafrański, K. Rećko, W. Olszewski, D. Satuła, P. Butkiewicz, and K. R. Szymański, Heat capacity anomaly near magnetic phase transition in $GaFeO_3$, J. Magn. Magn. Mater. **548**, 168978 (2022).

[23] K. Szymański, W. Olszewski, P. Butkiewicz, M. Biernacka, D. Satuła, K. Rećko, and M. Szafrański, Mössbauer measurements of $GaFeO_3$ single crystal multiferroic Hyperfine Interact. **242**, 26 (2021).

[24] CRYSALISPRO, Agilent.

[25] G. M. Sheldrick, SHELXT—Integrated space-group and crystal-structure determination Acta Crystallogr., Sect. A **71**, 3 (2015).

[26] See Supplemental Material at http://link.aps.org/supplemental/10.1103/PhysRevB.108.195101 for a detailed description of the algorithm governing the upper limit of the distance between paired atoms and a comprehensive list of atomic shifts.

[27] K. M. Rabe, C. H. Ahn, and J. M. Triscone, *Physics of Ferroelectrics* (Springer-Verlag, Berlin, 2007).

[28] P. E. Blöchl, Projector augmented-wave method, Phys. Rev. B **50**, 17953 (1994).

[29] J. P. Perdew, K. Burke, and M. Ernzerhof, Generalized gradient approximation made simple, Phys. Rev. Lett. **77**, 3865 (1996).

[30] G. Kresse and J. Hafner, *Ab Initio* molecular-dynamics simulation of the liquid-metalamorphous-semiconductor transition in germanium, Phys. Rev. B **49**, 14251 (1994).

[31] G. Kresse and J. Furthmüller, Efficient iterative schemes for *ab initio* total-energy calculations using a plane-wave basis set, Phys. Rev. B **54**, 11169 (1996).

[32] G. Kresse and D. Joubert, From ultrasoft pseudopotentials to the projector augmented-wave method, Phys. Rev. B **59**, 1758 (1999).

[33] J.-Y. Kim, T. Y. Koo, and J.-H. Park, Orbital and bonding anisotropy in a half-filled $GaFeO_3$ magnetoelectric ferrimagnet, Phys. Rev. Lett. **96**, 047205 (2006).

[34] F. Ibrahim and M. Alouani, Impact of excess iron on the calculated electronic and magnetic properties of gallium ferrite, Phys. Rev. B **85**, 174411 (2012).

[35] H. J. Monkhorst and J. D. Pack, Special points for Brillouin-zone integrations, Phys. Rev. B **13**, 5188 (1976).

[36] H. M. Petrilli and P. E. Blöchl, Electric-field-gradient calculations using the projector augmented wave method, Phys. Rev. B **57**, 14690 (1998).

[37] P. Pyykkö, Year-2017 nuclear quadrupole moments, Mol. Phys. **116**, 1328 (2018).

[38] K. Szymański, Polarized radiation in Mössbauer spectroscopy, Phys. Rep. **423**, 295 (2006).

[39] J. M. Greneche and F. Varret, A new method of general use to obtain random powder spectra in ^{57}Fe Mössbauer spectroscopy: The rotating-sample recording, J. Phys. Lett. **43**, 233 (1982).

[40] N. Blaes, H. Fischer, and U. Gonser, Analytical expression for the Mössbauer line shape of ^{57}Fe in the presence of mixed hyperfine interactions, Nucl. Instrum. Methods Phys. Res., Sect. B **9**, 201 (1985).

[41] A. L. Kholkin, D. A. Kiselev, and A. Heredia, Piezoresponse force microscopy, in *Encyclopedia of Materials: Science and Technology* (Elsevier, Amsterdam, 2011), pp. 1–8.

[42] D. Nečas and P. Klapetek, GWYDDION: An open-source software for SPM data analysis, Cent. Eur. J. Phys. **10**, 181 (2012).

[43] P. Gutlich, E. Bill, and A. X. Trautwein, *Mossbauer Spectroscopy and Transition Metal Chemistry. Fundamentals and Applications* (Springer, Berlin, 2011).

[44] E. König, R. Schnakig, and S. Kremer, Ligand-field spin-orbit energy levels in the d^5 electron configuration of octahedral and tetrahedral symmetry, Z. Naturforsch., A: Phys. Sci. **29**, 419 (1974).

[45] M. J. Han, T. Ozaki, and J. Yu, Magnetic ordering and exchange interactions in multiferroic $GaFeO_3$, Phys. Rev. B **75**, 060404(R) (2007).